Tellus SERIES A DYNAMIC METEOROLOGY AND OCEANOGRAPHY
PUBLISHED BY THE INTERNATIONAL METEOROLOGICAL INSTITUTE IN STOCKHOLM

A possible generation mechanism for internal waves near the edge of a submesoscale eddy

By I.P. CHUNCHUZOV[1]*, O.M. JOHANNESSEN[2], and G.O. MARMORINO[3], [1]*Obukhov Institute of Atmospheric Physics, Moscow, Russia;* [2]*Nansen Scientific Society, Bergen, Norway;* [3]*Remote Sensing Division, Naval Research Laboratory, Washington, DC, USA*

(Manuscript Received 11 May 2021; in final form 21 June 2021)

ABSTRACT

Recently, it has been shown for the first time by observations that an anticyclonic mesoscale eddy can generate internal waves (wavelengths of 0.4 to 1 km) that carry energy away from the eddy. In the present study, we investigate a possible mechanism for generating internal waves near the edge of a submesoscale eddy. The study was motivated by airborne infrared imagery that shows curved thermal bands (wavelengths ~70 m) near the edge of a 1-km-diameter cyclonic eddy. We hypothesize that these bands represent internal wave wakes generated by turbulent perturbations having scales of a few tens of meters that are advected along the eddy's thermal perimeter. An analytical theory is developed to investigate this for an idealized perturbation advected by a circular current. Calculations show that, for a reasonable choice of parameter values, an internal wave wake develops around the eddy that has spiral-like phase lines resembling the orientations and wavelengths of the field observations. The general validity of our proposed mechanism should be verified with further studies.

Keywords: submesoscale eddy, internal waves, thermal bands, spiral-like phase lines

1. Introduction

Internal waves in the ocean generated by tides, current flows over bottom topography, wind and oceanic fronts are well known phenomena playing an important role in ocean circulation, mixing and formation of the space-time spectra of fluctuations in temperature, salinity, density and current velocity (e.g., Miropolsky 2001; Alford 2003; Wunsch and Ferrari 2004; Taylor and Sarkar 2007; Molemaker et al. 2010; Shakespeare et al. 2014; Nagai et al. 2015; Shakespeare 2019). Some of the mechanisms of generation of internal waves still remain obscure including the mechanism of eddy dissipation in an un-balanced flow (Wunsch and Ferrari 2004). However, earlier Plougonven and Zeitlin (2002) developed a theory, where a pancake-like vortex of elliptic shape permanently radiated internal waves by the balanced but nonstationary vortex motion. Barkan et al. (2017) simulated numerically the low-frequency wind forcing (LFW) of an ocean jet which generated a mesoscale anticyclonic eddy of about 50 km scale along with midsize eddies. The energy transfer from large-scale motions to higher frequencies and smaller scales was simulated as well. Their results (Fig. 3 in Barkan et al. 2017) show a vertical velocity field dominated by spiral-like filaments (spacings of 3–4 km) that can be interpreted as internal waves radiating from the single, large anticyclonic eddy. This process can be clearly seen in a video produced by R. Barkan (J. McWilliams, personal communication 2021).

There are, however, few field experiments designed to explore if mesoscale eddies can directly generate internal waves in the ocean. An exception was the dedicated eddy-internal wave experiment in the marginal ice zone in the Greenland Sea: MIZEX 87 (Johannessen et al. 2019), where it was shown for the first time that an anticyclonic eddy with a scale of 40 km generated internal waves with a period of 1–3 cycle per hour (cph), an amplitude of vertical displacements up to 15 m, propagating away from the eddy with a group speed of 0.2 m/s. This integrated experiment included two aircrafts instrumented with Synthetic Aperture Radar (SAR), a triangular array of thermistors deployed on the drifting ice, including a current meter string and measurements of temperature and salinity profiles, and accompanied by meteorological observations from two research vessels (Johannessen et al., 1994).

*Corresponding author. e-mail: igor.chunchuzov@gmail.com

Citation: Tellus A: 2021, **73**, 1947610, https://doi.org/10.1080/16000870.2021.1947610

SAR images can observe both eddies and internal waves, an example of this being a SAR image of an eddy of 5-km scale, which radiated internal waves having wavelengths from a few hundred meters up to 1000 m in an area North of Svalbard (Sandven and Johannessen 1987; their Fig. 1, lower-left corner). Actually, it was this SAR image which led Johannessen et al. (2019) to propose the hypothesis that internal waves could be generated by eddies and to perform the eddy-internal wave experiment as part of MIZEX 87.

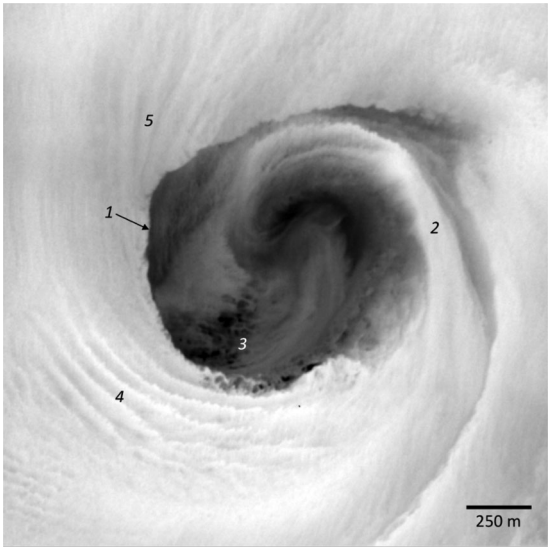

Fig. 1. Infrared image of a cyclonic cold-core eddy, located near the island of Santa Catalina, California, as described in Marmorino et al. (2018). Temperature range is approximately 1 °C and spatial resolution is 3 m. Indicated are the eddy thermal perimeter (1); a sector of warm inflow (2); small-scale cold patches (3); and areas of persistent banding (4, 5).

SAR images from space cannot resolve small-scale physical structures of the order of 10 m, as might occur in association with much smaller eddies. That level of detail can, however, be investigated using high-resolution thermal imagery as collected by an airborne infrared (IR) camera. An example is shown in Fig. 1. It is from a field study by Marmorino et al. (2018) of a cold-core submesoscale eddy formed just downstream of Santa Catalina, a deep-water island located off the coast of California. The eddy diameter is about 1 km and its rotation is cyclonic, with a maximum swirling speed of 0.3 to 0.4 m/s occurring near the thermal perimeter of the eddy. The Rossby number was very high, with a value of 27, thus indicating the importance of the centrifugal force and pressure gradient in the submesoscale eddy dynamics. Strong radial flows occur too: warm-water inflow on the right-hand side of the eddy; elsewhere, outward flow of cooler water toward the eddy perimeter. Also, evidence of turbulent mixing, both within the eddy and along its perimeter, occurs as small cold patches, which are discussed further, below.

The most significant feature in Fig. 1 for the present study is the occurrence of two groups of five or so thermal bands, lying in the warmer water but having the appearance of curving away, or diverging, from the thermal perimeter of the eddy. The mean spacing between bands is about 70 m. The clearer group of bands (feature

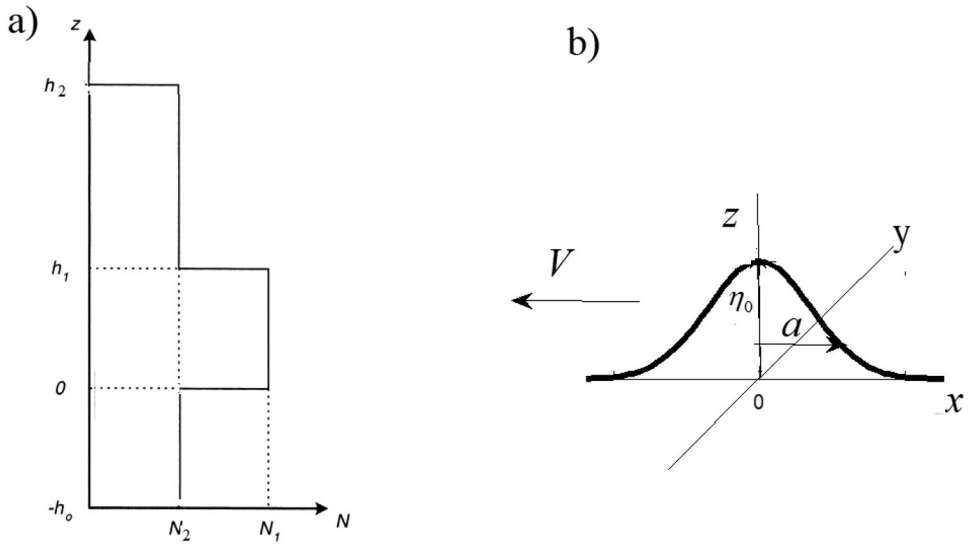

Fig. 2. (a) A model of the vertical profile of the BV-frequency $N(z)$ in the ocean. The layer $0 < z < h_1$ represents the thermocline, which has a maximum BV-frequency $N_1 \gg N_2$. (b) An idealized perturbation to the thermocline (at $z = 0$), having a vertical displacement $z = \eta(x + Vt, y)$ and characteristic horizontal scale a. The perturbation is shown moving to the left at velocity V.

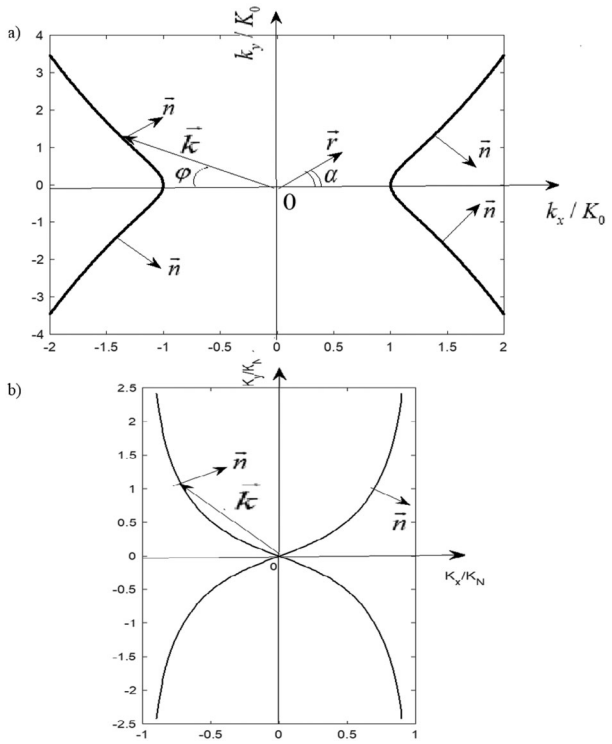

Fig. 3. Wave number curves relating wave number components k_x and k_y of the wave number vector $\vec{k}$ of stationary internal waves generated by a horizontally moving (to the left) source with speed V. (a) Case of the thin stably stratified layer with $N = N_1$ inside the deep water ($\mu_1 h_1 \ll 1,\ kh_0 \gg 1, k\Delta h \gg 1$). (b) Case of the stably stratified layer in the shallow water ($k\Delta h \ll 1$ and $\mu_2 h_0 \ll 1$).

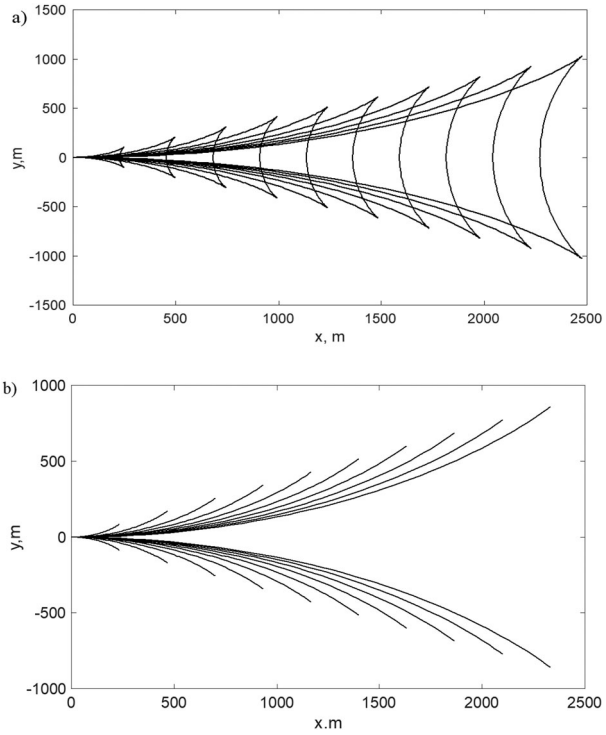

Fig. 4. Calculation of constant phase lines for different $m = 1, 2, \ldots, 10$ at some time t, when the source was at the origin, and the ten wave crests shown here were radiated by the source at previous times. (a) The case when the horizontal dimensions of the source a=30-100 m, and the directions $\vec{k}$ of the propagation of wave crests with respect to the direction of the source velocity lie in the interval $|\varphi| < \pi/2$. (b) The horizontal dimension a=10 m, and the interval of $\vec{k}$-directions is $\pi/4 < |\varphi| < \pi/2$.

4 in Fig. 1) persisted essentially unchanged over the 40 min sampling period and were fixed in position relative to the eddy. Our hypothesis is that these thermal bands are internal waves generated by the eddy. An analytical theory is developed in section 2 to investigate how this might occur; sample calculations are performed, using parameter values based on the field study, and results are compared with the IR image. Section 3 discusses the results and conclusions are given in section 4.

2. Modeling eddy-generated internal waves

An essential part of our hypothesis is the existence of a "ducting" layer for internal waves. In the present case, this is a thin thermocline transitional layer, separating a near-surface layer of warm water and a lower layer of cold water, that has high static stability (Brunt-Väisälä frequency of about 19 cph, see below) and is also close to the surface. A second key assumption is the occurrence of density perturbations, created through the action of vertical turbulent mixing. Such mixing is presumed to have created the cold patches in Fig. 1. These patches, which arise from hydrodynamic instabilities induced by either vertical or horizontal current shear, have a dominant scale of 10 to 15 m, though larger patches can also be seen that presumably form through a merging of smaller ones. Shear is presumed to be large especially along the eddy perimeter, where the flow, having both swirling and (outward) radial velocity components, subducts beneath the warm layer external to the eddy core. Outward radial flow also results in surface flow convergence along the eddy perimeter (Marmorino et al. 2018, their Fig. 4a); this induces vertical flow that can directly lead to nonstationary vertical displacements of the thermocline layer and generate internal waves. It can also be seen in the IR imagery that there is spatially periodic structure within the eddy; and as this is advected by radial flow into the eddy perimeter, it may also act as an internal wave-generator.

Based on the observed current and temperature structure of the submesoscale eddy, we assume that the patches of different temperature (equivalently, density),

moving with the maximum circular current speed of 0.3–0.4 m/s along the eddy perimeter relative to the surrounding water, cause nonstationary perturbations in the radial velocity of the current near the eddy perimeter and vertical velocities in the stably stratified thermocline layer. Such local nonstationary perturbations propagate away from the perimeter as internal waves (e.g., Lighthill 1978; Miropolsky 2001). In other words, the temperature (or density) irregularities advected by circular current inside the eddy at its perimeter can be considered as moving sources of internal wave wakes seen as the banded structure around the perimeter of the eddy (Fig. 1). Below we attempt to explain our hypothesis.

2.1. Internal wave wakes generated by a horizontally moving source

Consider now a temperature inhomogeneity moving with a current speed V along the perimeter of a cyclonic eddy relative to the surrounding stably stratified water near the perimeter. The inhomogeneity causes – at each fixed point in space with coordinates x, y, z – small nonstationary temperature perturbations $T'(x, y, z, t)$ relative to the undisturbed temperature of the medium $T_0(z)$, which depends on the depth z. The temperature perturbations in a stably stratified and incompressible medium with the square of the Brunt-Väisälä (BV) frequency $N^2(z) = -g{\rho_0}^{-1}d\rho_0/dz$, where $\rho_0(z)$ is the unperturbed density of the medium, cause the density perturbations $\rho'(x, y, z, t)$ and vertical displacements $\eta(x, y, z, t)$ of the fluid particles, related by the following equation (Gossard and Hooke 1975):

$$\frac{\rho'}{\rho_0} = \frac{N^2}{g}\eta, \tag{1}$$

obtained from the linearized continuity equation for an incompressible fluid, $\frac{\partial \rho'}{\partial t} + w\frac{d\rho_0}{dz} = 0$, where $w = \frac{\partial \eta}{\partial t}$ is vertical velocity, and $\vec{V}$ is the horizontal velocity of the inhomogeneity.

In the case when unsteady displacements of the fluid in some fixed volume of space are caused by the passage through it of a temperature (or density) inhomogeneity moving with a constant velocity, then such inhomogeneity may generate internal wave wakes like a moving body in the stably stratified fluid (Lighthill 1978, their Sec. 4.12). The spatial structure of the internal wave field generated by such a source depends on the ratio of the group speed of these waves to the speed of the moving source (Lighthill 1978).

When the source speed is greater than the group speed of the internal waves, then the shape of the internal wave crests diverging from their source at the pycnocline are similar to that of surface wave crests diverging from the bow of a straight moving ship, the so-called Kelvin ship waves (Thomson 1887; Lighthill 1978; Tunaley 2012). Such internal wave wakes were also generated at the pycnocline of the two-layer system in the Arctic Ocean by ice pressure ridge keels underneath the pack ice (Morison 1986).

In the case we consider here, we will first study the form of the wave crests diverging from a source moving in a straight line and then generalize their form to the case of a source moving in a circle.

Let us consider the structure of the internal wave field generated by a source of finite size moving horizontally to the left (opposite to the direction of the x-axis) with a constant velocity $\vec{V} = (-V, 0, 0)$ (Fig. 2b) in a stably-stratified fluid with BV- frequency $N(z)$ (Fig. 2a). The BV-frequency profile $N(z)$ in the ocean is often described by a three-layer model shown in Fig. 2a, with the ocean surface at$z = h_2$, the maximum $N(z)$=N_1 in the thermocline layer at $0 \le z \le h_1$, and the bottom at $z = -h_0$ (Brekhovskikh and Goncharov 1994; their Sec. 40).

Let us set the vertical displacement at the lower boundary ($z = 0$) of the layer with a maximum of $N(z)$ as follows:

$$\eta(x, y, z = 0, t) = \eta_0 f(x + Vt, y) \tag{2}$$

where function $f(x, y)$ describes the shape of the displacement surface, η_0 is the displacement maximum, and a is the characteristic horizontal scale of the area within which the displacement is localized in the thermocline layer.

Marmorino et al. (2018, their Fig. 5b) observed a sharp decrease in density with increasing z in a thermocline layer of thickness h_1~5–10 m. The non-dimensional density jump $\Delta\rho/\rho$ over the layer thickness Δz=h_1 was about -6×10^{-4}; hence the maximum BV-frequency $N_1 \approx \left(-g\rho^{-1}{}^{\Delta\rho}/_{\Delta z}\right)^{1/2}$ in this layer was in the range 0.024–0.033 rad/s or 13.75–18.91 cph. Given that the vertical displacement η of an incompressible fluid particle due to its relative density perturbation, $\rho'/\rho \sim \Delta\rho/\rho = -6 \times 10^{-4}$, is determined from (1), we obtain that the maximum displacement $\eta_0 \sim |\rho'/\rho|/({N_1}^2/g) \sim$5–10 m. Thus, from (2) it follows that vertical fluid velocity $w(x, y, z, t)$ at $z = 0$ is

$$w(x, y, z = 0, t) = {}^{\partial\eta}/_{\partial t} = V\eta_0 \partial f/\partial x, \tag{3}$$

and its amplitude $w_0 \sim V\eta_0/a$.

The temperature irregularities at the eddy's periphery have horizontal scales a from 10 to 50 m. They are advected along the perimeter with a maximum speed V=0.3–0.4 m/s, where the speed V rapidly drops in the transverse direction to less than 0.2 m/s when moving away from the perimeter (Marmorino et al. 2018, their

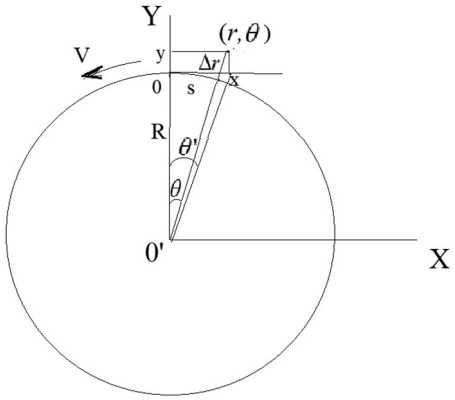

Fig. 5. Diagram of transition from rectangular coordinate system (x,y) to the local curvilinear coordinate system (r,θ) near the perimeter of the circle.

Fig. 6a). Taking into account that the speed V of the temperature irregularities near the perimeter of the eddy is in the range $V=0.15$-0.3 m/s, and choosing $\eta_0=5$ m and $a=50$ m, then the amplitude w_0 of the vertical velocity perturbed by the temperature irregularity is in the range 0.015-0.03 m/s.

Let us now transfer to a reference frame moving to the left along with the wave source by replacing in (3) the variables $x' = x + Vt$, $y'=y$. Then, the problem of finding the vertical velocity field $w(x', y, z)$ in the stratified fluid with a profile $N(z)$ in Fig. 2a and the boundary condition $w(x', y, z = 0) = V\eta_0 \partial f/\partial x'$ becomes equivalent to the problem of finding the perturbations of the stably stratified current (directed along the x-axis) when flowing around an obstacle like mountain (Lighthill 1978, their Sec. 4.12; Gjevik and Marthinsen 1978; Chunchuzov et al. 2000).

This problem can be solved by a Fourier transform of the field $w(x', y, z)$ and the boundary condition $w(x', y, 0)$ on to harmonic plane waves

$$w(x', y, z) = \int dk_x \int dk_y \tilde{W}(k_x, k_y, z) \exp(ik_x x' + ik_y y), \tag{4}$$

where $\tilde{W}(k_x, k_y, z)$ is the Fourier transform of $w(x', y, z)$. Substituting (4) into the equation for internal wave field $w(x', y, z)$ in the Boussinesq approximation (Lighthill 1978; Sec. 4.1) leads to the Helmholtz equation for $\tilde{\mathbf{W}}(k_x, k_y, z)$:

$$\mathrm{d}^2\tilde{\mathbf{W}}(k_x, k_y, z)/\mathrm{d}z^2 + k^2(N^2/\omega'2-1)\tilde{\mathbf{W}}(k_x, k_y, z) = 0 \tag{5}$$

with the boundary condition

$$\tilde{\mathbf{W}}(k_x, k_y, z = 0) = ik_x V\tilde{f}(k_x, k_y), \tag{6}$$

where $\tilde{f}(k_x, k_y)$ is the Fourier transform of the displacement field (2) at $z=0$, $k^2 = k_x{}^2 + k_y{}^2$, and

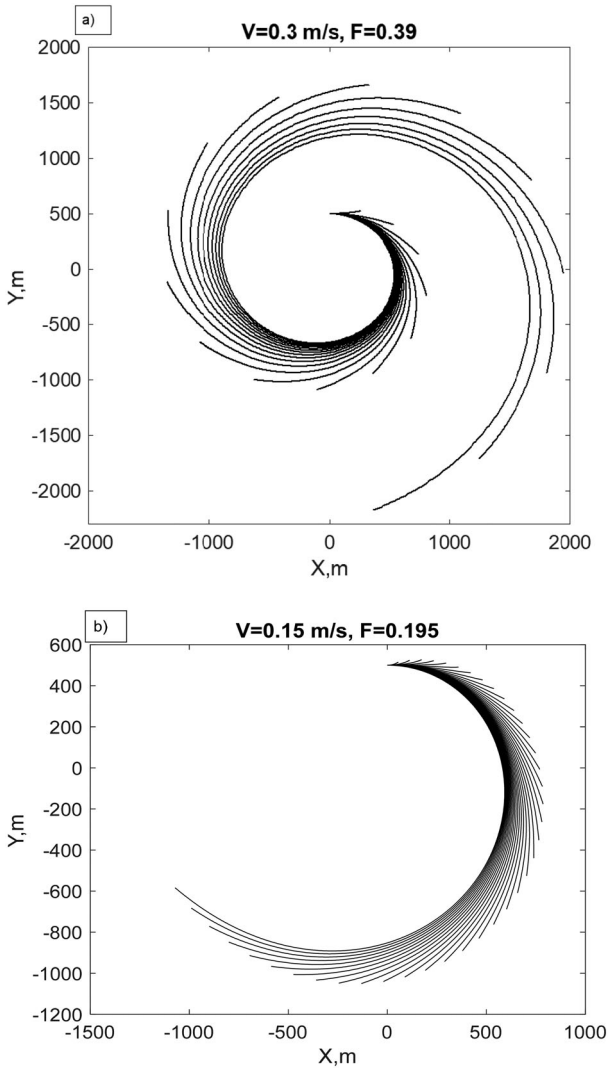

Fig. 6. Spiral-like wave phase lines behind a point source at arbitrary moment t in two cases: (a) $V=0.3$ m/s, $a=10$ m, Froude number $\mathrm{F}=0.39$, $m=1,2,\ldots,20$; (b) $V=0.15$ m/s, $a=10$ m, $\mathrm{F}=0.195$,$m=1,2,\ldots 40$. Case (a) is a better match to field observations (see Fig. 7), and in this case the wave source has traveled 5 km in 4.63 h, or 1.6 revolutions. Over time, the source together with the entire pattern of phase lines behind it rotates in a counterclockwise circle with velocity V.

$$\omega' = -k_x V \tag{6A}$$

is the wave angular frequency relative to the ground.

The solution of the boundary problem (5)–(6) with the conditions of equality $\tilde{\mathbf{W}}(k_x, k_y, z)$ to zero on the bottom $z=-h_0$ and on the ocean surface $z=h_2$ (the so-called "hard cover" approximation), and with a condition of continuity of the vertical velocity and its derivative on z at the inner boundaries between the layers, leads to the following dispersion equation for eigenvaluesk_n, $(n=1,2,.,)$ (Brekhovskikh and Goncharov 1994):

$$\tan(\sigma) = P(\sigma),\ N_2^2 < \omega'^2 \le N_1 \tag{7}$$

$$P(\sigma) = \frac{k^{-1}\mu_1\left[\mathrm{th}(k\Delta h) + k\mu_2^{-1}\mathrm{th}(\mu_2 h_0)\right]}{\left[k^{-1}\mu_1^2\mu_2^{-1}\mathrm{th}(k\Delta h)\mathrm{th}(\mu_2 h_0) - 1\right]}, \tag{8}$$

where

$$\sigma=\mu_1 h_1, \mu_1=k(N_1^2/\omega'^2-1)^{1/2}, \mu_2=k(1-N_2^2/\omega'^2)^{1/2}, \quad \Delta h=h_2-h_1 \tag{9}$$

$$\omega'=-k_x V=-kV\cos(\psi), \tag{10}$$

and ψ is the angle between vector $\vec{k}=(k_x,k_y)$ and direction of the x-axis. Equations (7)-(8) determine the discrete horizontal wave numbers $k_n(\psi)$ of normal modes with $n=1,2\ldots$, trapped in the layer of maximum stability with-$N=N_1 \gg N_2$. The wave field (4) can be found by taking the residues at $k=k_n(\psi)$ of the under integrand expression in (4), written in cylindrical variables k and ψ, and then using far from the source a stationary phase method over ψ (see Lighthill 1978; Chunchuzov et al. 2000). Inside the layer with $N=N_1$ the mode amplitudes $\left|\tilde{W}_n(z)\right|$ oscillate with changing vertical co-ordinate z, but decrease as we move away from this layer to the lower layer ($-h_0<z<0$) and to the upper layer ($z>h_1$).

2.1.1. Case (a): a thin stably stratified layer in deep water *($\mu_1 h_1 \ll 1$, $kh_0 \gg 1, k\Delta h \gg 1$)*. In the specific case of weak stratification of the lower and upper layers, $N_2^2 \ll \omega'^2 < N_1^2$, we can take $\mu_2 \approx k$. In addition, we will assume that $k\Delta h \gg 1$ and $kh_0 \gg 1$, so that the amplitudes of trapped modes decrease rapidly with increasing z in the upper and lower layers. In this case for the thin layer ($\mu_1 h_1 \ll 1$) with the high value of N, after certain approximations we obtain the following equation (Eq. 4A in the Appendix)

$$V^2 k_x^2 = g\varepsilon k/2 \tag{11}$$

where $\varepsilon \equiv -\Delta\rho/\rho$ is the absolute value of the relative density jump within the thin layer with $N = N_1$.

The Eq. (11) is analogous to the dispersion equation for the stationary ship waves in deep water relating horizontal wave numbers k_x and k_y (Lighthill 1978, their Sec. 4.12, Eq. 445), in which the acceleration of gravity g is replaced by $g\varepsilon/2$ in Eq. (11).

The wave number components satisfying Eq. (11) describe a dispersion wave number curve shown in Fig. 3a. These components are normalized to the minimum wave number of internal waves $K_0 \equiv g\varepsilon/(2V^2)$ in the thin stably stratified layer. If we choose an arbitrary direction $\vec{r}$ from the origin of the co-ordinate system to the observation point (x,y) with an angle α to the x-axis, then in this direction we can detect only those waves which have wave number vector $\vec{k}$ (Fig. 3a), the end of which lies at the point of the wave number curve, at which the normal $\vec{n}$ is parallel to the direction $\vec{r}$. For different directions α from the source we can find the wave components with the corresponding local wave numbers $\vec{k}$ that shape together a wave packet.

Fig. 7. Overlay of calculated phase lines (from Fig. 6a) on the infrared image from Fig. 1. The spiraling phase lines resemble the shape and wavelength of the banded structures in the image.

From the shapes of the wave number curves, it can be seen that all the $\vec{n}$-directions at the points on these curves lie within a wedge with the half-width angle α determined by the inflection points of the curves (where α reaches a maximum) . The forms of the lines $r = r(\varphi)$ of constant phase (wave crests and troughs) corresponding to the wave number curves are determined from the condition $\vec{k}(\varphi)\vec{r} = (\vec{k}(\varphi)\vec{n})r$=const, where φ is the angle between the wave number vector $\vec{k}(\varphi)$, depending on a given angle α of the observation point, and the direction of motion of the source (toward the negative values of the x-axis). Therefore, the shapes of the lines of constant phase $r(\varphi) =$ const$/(\vec{k}(\varphi)\vec{n})$ are determined by the dependence on φ of the projection of the wave number vector $\vec{k}(\varphi)\vec{n}$ on to the directions of normal $\vec{n}$ at the points of the wave number curve.

The equations describing constant phase lines (wave crests and troughs) for internal waves in a thin stably stratified layer that is above a lower layer of arbitrary thickness h_0 can be presented in the following parametric form (Gjevik and Marthinsen 1978):

$$x_m = 2\pi m h_0 F^2 \cos^3(\varphi)\left[1-F^2\cos^2(\varphi)+2\tan^2(\varphi)\right] \times\left[1-F^2\cos^2(\varphi)\right]^{-2}, (m=1,2,3\ldots) \tag{12}$$

$$y_m = -x_m \tan(\varphi)[1+F^2\cos^2(\varphi)][[1-F^2\cos^2(\varphi) + 2\tan^2(\varphi)]^{-1}, (-\pi/2<\varphi<\pi/2) \tag{13}$$

where $F = V/(g\varepsilon h_0)^{1/2}$ is the Froude number in the lower layer of thickness h_0.

For $\varepsilon = 6 \times 10^{-4}$, h_0=100 m, V=0.3 m/s the Froude number F=0.39. Figure 4a shows the constant phase lines for $m = 1, 2, \ldots, 10$ at some arbitrary time t, when the source was at origin, and ten wave crests were radiated by the source at previous times. This pattern of wave crests is stationary with respect to the source (i.e. has a zero intrinsic phase speed and zero frequency) and propagates as a whole with the source to the left with the speed V.

In the direction α from the source to the observation point the local wavelength $\lambda = 2\pi/k(\varphi)$ depends on the angle $\varphi(\alpha)$ depending on α, but the amplitude wave number spectrum $|\tilde{W}|$ of the vertical velocity is proportional to the amplitude spectrum of the source $|k\cos(\varphi)V\tilde{f}(k_x(\varphi), k_y(\varphi))|$. For the displacement $f(x, y)$ (at the boundary $z = 0$) with horizontal scale a and axisymmetric wavenumber spectrum $\tilde{f}(k)$ proportional to $\exp(-ka)$, the vertical velocity spectrum $|\tilde{W}|$ has a maximum at wave number $k(\varphi) \sim a^{-1}$, so the maximum wave energy corresponds to the wavelengths $\lambda \sim 2\pi a$. On the other hand, according to condition (7), the internal waves are trapped in the layer with $N = N_1$ only in the case when $|k(\varphi)V\cos(\varphi)| \sim |V\cos(\varphi)/a| < N_1$. For example, if $a \sim$30-100 m, then the latter condition is satisfied for the entire range $|\varphi| < \pi/2$, and the pattern of constant phase lines (e.g., wave crests) is as shown in Fig. 4a; but for small irregularities, which have $a \sim$10 m, condition (7) is satisfied only for the interval $\pi/4 < |\varphi| < \pi/2$, for which the pattern of wave crests is as shown in Fig. 4b. Their maximum amplitudes are reached at wavelengths $\lambda \sim 2\pi a = 63$ m.

2.1.2. Case (b): a stably stratified layer in shallow water *($k\Delta h \ll 1$* and *$\mu_2 h_0 \ll 1$)*. Let us consider now another case, when the layers above and under the stably stratified layer with $N(z) = N_1$ are thin, $k\Delta h \ll 1$ and $\mu_2 h_0 \ll 1$, so that the value of the right side (8) of the Eq. (7) is small: $|P(\sigma)| \ll 1$. In this case, the approximate solutions of Eq. (7) are:

$$\sigma_n \approx \pi n, n = 1, 2.... \tag{14}$$

From (9)–(10) and (14) we obtain the following equations

$$(k_x{}^2 + k_y{}^2)\left(\frac{N_1{}^2}{k_x{}^2 V^2} - 1\right) h_1{}^2 = \pi^2 n^2, \tag{15}$$

which, after designating $k_N = N_1/V$, $C_n = N_1 h_1/(\pi n)$, and $M_n = V/C_n$, can be rewritten in the nondimensional form

$$Y^2 = M_n{}^2 X^2 (1 - X^2)^{-1} - X^2, \tag{16}$$

where $X = k_x/k_N$ and $Y = k_y/k_N$. The Eq. (16) describes a set of the wavenumber curves $Y = Y_n(X)$, corresponding to the wave modes with $n = 1, 2, \ldots$. and phase speeds $C_n = N_1 h_1/(\pi n)$ in the hydrostatic approximation (Brekhovskikh and Goncharov 1994). For $M_n > 1$ the wavenumber curve for the first mode ($n = 1$) is shown in Fig. 3b. This curve describes the diverging wave crests, like those shown in Fig. 4b, confined within the wedge with a semi-angle equal to $\pi/2 - \arctan(M_m{}^2 - 1)^{1/2}$. If we take N_1=0.024 rad/s and h_1=5 m, then $C_1 = N_1 h_1/\pi$=0.076 m/s and M_1=3.93 for the first mode with $n = 1$, giving a wedge semi-angle of about 15°.

We have thus shown that both for the deep and shallow water approximations, the internal ship waves in the layer with a maximum $N = N_1$ have diverging wave crests within a wedge like those shown in Fig. 4b (in which only diverging crests present and no transverse or stern waves).

The internal waves generated by moving inhomogeneities induce spatial and temporal variations in the current velocity field within and outside the eddy. The current velocity disturbances caused by trapped waves in the layer with $N = N_1$ can be estimated for the case, $k\Delta h \ll 1$ and $\mu_2 h_0 \ll 1$, when this layer is close to the surface and bottom. With increasing distance $r = (x^2 + y^2)^{1/2}$ from the source the wave amplitude decreases as $r^{-1/2}$, therefore, if the amplitude of the vertical displacements is 5 m at a distance $r \sim$60 m from the source, then it will be about 1.7 m at a distance $r \sim$500 m. According to (3) the vertical velocities w are 0.015-0.03 m/s near the source, and ~ 0.005-0.01 m/s at a distance $r \sim$500 m from it.

At large distance ($r \gg a$, $kr \gg 1$) from the source we can also estimate the horizontal velocity perturbations v_x' and v_y' caused by internal waves. In the arbitrary direction α of the radius-vector $\vec{r}$ from the source to the observation point within the wedge we can find the components of the wave packet with local wave number vector $\vec{k}(\alpha) = (k_x, k_y)$. Using the polarization equation $v_x'/v_y' = k_x/k_y$, which is obtained from the linearized Euler equations for v_x' and v_y', and the continuity equation $\partial v_x'/\partial x + \partial v_y'/\partial y = -\partial w/\partial z$ we can estimate the amplitude of the horizontal velocity perturbations $v = (v_x'2 + v_y'2)^{1/2}$ from the continuity equation: $kv = -\partial w/\partial z$, where $k = \left|\vec{k}(\alpha)\right|$ is the magnitude of the local wavenumber vector $\vec{k}(\alpha)$. For the lowest mode ($n = 1$): $\partial w/\partial z \approx \pi h_1{}^{-1} w$, therefore $v \sim \pi(kh_1)^{-1} w$, which for $h_1 \sim$10 m, $k = a^{-1} \sim 10^{-1}$ rad/m, and w = 0.01 m/s at a distance r = 500 m from the source gives the amplitude of the horizontal velocity oscillations $v \approx$ 0.03 m/s. For the diverging phase lines like those shown in Fig. 4b the total current velocity field $\vec{V} + \vec{v}$ perturbed by internal waves has a nonzero horizontal divergence.

2.2. *Spiral-like crests of internal waves*

We now return to consider an internal wave field generated by a thermocline perturbation advected with velocity

V along a circular path having radius R. From the field measurements, we choose $V = 0.3$ m/s and $R = 500$ m, which is very much larger than the perturbation scale length a.

Let the source be at an arbitrary moment t at the beginning of the coordinate system x,y shown in Fig. 5, and the pattern of wave crests behind the source looks like that in Fig. 4b. We transform the coordinates (x,y) of an arbitrary point located at a small distance from the perimeter of the circle ($|y| \ll R$) to its curvilinear coordinates (r, θ) shown in Fig. 5 using a variable transform:

$$r = R + \Delta r \approx R + y, \quad \theta \approx \theta' = x/R, \tag{17}$$

where we have taken into account that in a narrow ring $\Delta r \ll R$ near the perimeter and at a small angle θ, where the wave field is concentrated, the arc length corresponding to the angle θ is $s \approx x$, and $\Delta r \approx y$.

To obtain the form of the wave phase lines in the curvilinear coordinate system (17), we substitute $x = x_m, y = y_m$ from the system of equations (12)-(13) into (17) considering the case of the diverging waves in Fig. 4b. Then the equations of wave phase lines with $m = 1,2,\ldots$ will take the following parametric form:

$$X(\theta_m) = r\sin\theta = (R + y_m)\sin\theta_m, \tag{18}$$

$$Y(\theta_m) = r\cos\theta = (R + y_m)\cos\theta_m, \theta_m = x_m/R \tag{19}$$

The shapes of the phase lines, described by (18)-(19), outside the perimeter of the circle ($r>R$) are shown in Fig. 6a, b for the cases $V = 0.3$ m/s and $V = 0.15$ m/s, respectively. The phase lines inside the perimeter, $r<R$, are not shown here since we do not take into account changes in the shape of the phase lines inside the eddy core due to significant changes in the depth of the thermocline layer when approaching the center of the eddy, and also due to the strong decrease of the circular speed that affects refraction of the phase lines. We focus here on the banded structure outside of the perimeter to explain its appearance.

The phase lines outside the perimeter have a spiral-like shape, and for an arbitrary direction θ the local distance λ between neighboring phase lines increases with increasing r in the radial direction from the center of the circle. However, as mentioned above, the spectrum of wave energy has a maximum at wavelength $\lambda = 2\pi a$, which is 60-90 m for inhomogeneities of scale $a\sim$10–15 m. These λ values are comparable to the spacings of the IR bands (Fig. 1). The observed spiral shape of these bands allows us to suggest that they are the crests and troughs of internal waves, the mechanism of generation of which was described above.

It is seen from Fig. 6 that the case with $V = 0.3$ m/s (Fig. 6a) matches better with observations than Fig. 6b with $V = 0.15$ m/s. The match-up can be seen in Fig. 7, where the wave pattern in Fig. 6a has been superimposed on the infrared image of Fig. 1. The spiraling phase lines of the model resemble both the shape and wavelength of the banded structures in the image.

It should be noted that the small-scale internal waves with the wavelengths shorter than 10 m are comparable in their amplitudes to the displacements caused by all waves. This should lead to the wave-induced advection of each wave of the wave packet by the current perturbed by all the other waves and to the nonlinear steepening of the wave crests that may lead to the breaking down of such waves into small-scale turbulence (Chunchuzov 2018). The internal wave breaking processes associated with the wave-induced shear and convective instabilities can be one of the causes of the observed turbulent mixing between cold and warm waters at the eddy's perimeter.

The internal wave perturbations of the horizontal current velocity $\vec{v}$ are perpendicular to the diverging phase lines and this. as mentioned above, results in the non-zero horizontal divergence of the perturbed current velocity $\vec{V} + \vec{v}$ near the edge of the eddy. Such perturbations also cause quasi-periodic spatial variations in the current velocity field $\vec{V} + \vec{v}$ outside of the eddy perimeter.

The presence of a large number of inhomogeneities following each other along the eddy's perimeter may lead to the fact that one of the sources displaced from some position on the circle after a short period of time will be replaced by another similar source following the first one, and so on (Fig. 1). As long as such a process of replacement of one source by another is repeated, the internal wave pattern seen as a banded structure in some local area near eddy's edge will remain almost steady. The curved banded structure in the IR image (Fig. 1) does remain almost steady for at least 40 min, as may be seen from a video animation in Marmorino et al. (2018; Supplementary Material). It should be noted, however, that the internal waves emitted by the eddy can be expected to remove energy and angular momentum, thereby affecting the eddy's evolution over time (Plougonven and Zeitlin 2002).

3. Discussion

We considered a possible new mechanism for the formation of the banded structures observed on infrared images near the thermal perimeter of a submesoscale eddy studied in Marmorino et al. (2018). The detailed thermal structure of the eddy itself and its thermal perimeter separating cold and warm water masses seen in the images indicated a possible connection between the observed turbulent temperature inhomogeneities and the banded

structures near this perimeter, which we interpreted as internal wave wakes.

In the theory developed here it was shown that the advection of temperature inhomogeneities by the circulating eddy current leads to unsteady vertical displacements of the stably stratified thermocline layer with the maximum Brunt-Väisalla frequency value $N(z)$ (compared to the N values in the mixed near-surface ocean layer and the lower depth layer) and the generation of ducted internal gravity wave modes in this layer. The mechanism considered here complements that of permanent Lighthill radiation of internal waves by the balanced but nonstationary vortex motions in the elliptic pancake-like eddy (Plougonven and Zeitlin 2002).

It was also shown that the wave phase lines outside the thermal perimeter of the eddy have a spiral-like shape and increasing local wavelengths with increasing radial distance from the eddy center. For the temperature inhomogeneities with horizontal scales a=10–15 m the wave energy distribution over wavelengths have a maximum at wavelengths $\lambda = 2\pi a$, which were estimated to be in the range 60–90 m. Such scales are typical for the banded structures observed near the eddy's periphery. The observed spiral shape of these structures allowed us to suggest that they can be the crests and troughs of internal wave wakes generated behind the temperature irregularities advected by the cyclonic current near the thermal perimeter of the eddy.

The temperature inhomogeneities of different scales a seen in the IR image (Fig. 1) are randomly distributed along the eddy's perimeter and, therefore, cause random perturbations of the vertical velocity with some horizontal wavenumber spectrum $\left|\tilde{W}(k_x, k_y)\right|$. However, the condition $N_2{}^2 < \omega' 2 \leq N_1$ (see (7)) that provides the ducting of wave modes in the thermocline layer, selects only certain range of the wavenumbers $k \sim a^{-1}$ that obeys the condition $N_2{}^2/V^2 < k_x{}^2 \leq N_1{}^2/V^2$. This condition is well satisfied for the scale range $a = 10$–15 m of the inhomogeneities we have chosen above. Such a narrow scale range is filtered by the temperature stratification with certain $N(z)$-profile and leads to the generation of periodically spaced spiraling banding structures with wavelengths λ close to those observed in the IR image (Fig. 1).

The calculated pattern of internal waves is in reasonable agreement with the banded structure in the IR image (Fig. 7), but the image exhibits only part of the predicted spiral structure. There are several reasons for this. First, agreement can be expected mostly over the part of the spiral wake having wavelengths of 60 to 70 m, which correspond to the ducted modes excited by the maximum of the wavenumber spectrum of the inhomogeneities. Within this part of the wake the spacing does not vary significantly, and this prediction is consistent with what we see in the observed banded structure. The bands converging toward a point source are of much shorter wavelengths and as mentioned above should break down into turbulence due to wave-induced instabilities; hence, this part of the spiral wake might not exist in reality and cannot be observed in the image. Second, as to the part of the wave spiral with long wavelengths, which is far (on a circle arc) from the point source, the corresponding amplitudes of waves become so small as to be difficult to detect them.

The theoretical model developed here makes a number of simplifying assumptions. One is that it uses a purely circular flow to advect a density inhomogeneity with a local maximum speed at the eddy's perimeter relative to still, unperturbed stratified water outside of this perimeter. The real horizontal shear of the eddy is not taken into account. Another assumption is that the model uses as a source a single, hypothetical perturbation of fixed amplitude, although there are many such sources distributed along the perimeter of the observed eddy that contribute to the total internal wave field.

There is some analogy of our mechanism with the generation of atmospheric gravity waves by strong thunderstorms near the eye of a tropical cyclone (Nolan and Zhang 2017). In that case, convective cells existing in the thunderstorms produce upward and downward air motions that cause nonsteady vertical displacements in a stably stratified troposphere. These internal wave sources are advected by a circulating flow with a maximum speed near the core. The result is an outward radiation of waves that also assume a spiral shape, but it this case because of large differential advection of the sheared tangential flow. As found from the simulation by Nolan and Zhang (2017), the wave amplitudes can be related to the maximum wind speed in the core of the storm.

4. Conclusions

We have investigated a possible mechanism for generating internal waves near the edge of a submesoscale eddy. Our work was motivated by a field study (Marmorino et al. 2018) that showed persistent banding (wavelength ~ 70 m) around parts of a 1-km-diameter eddy, as well as 10–15 m wide density irregularities near the perimeter of the eddy (Fig. 1). It is suggested here that the banding results from an internal wave wake generated by inhomogeneities having scales of a few tens of meters that are advected along the eddy's thermal perimeter. The inhomogeneities cause nonstationary perturbations in the radial velocity of the current near the eddy's perimeter and vertical displacements in the thin layer of high static stability near the ocean surface. Such perturbations,

idealized here as a single source (Fig. 2), are shown analytically to generate internal wave wakes having spiral-like phase lines. These theoretical phase lines have orientations and wavelengths resembling those of the field observations (Fig. 7). The general validity of our proposed mechanism should be verified with further studies.

Acknowledgements

We thank J. C. McWilliams and R. Barkan for helpful discussions, and R. Davy for editorial comments.

Disclosure statement

No potential conflict of interest was reported by the authors.

Funding

The first author (IPC) was supported by the Russian Science Foundation grant №21-17-00021. OMJ was supported by Nansen Scientific Society; GOM was supported by the Office of Naval Research under NRL Project 72-1R25.

References

Alford, M. H. 2003. Redistribution of energy available for ocean mixing by long-range propagation of internal waves. *Nature* **243**, 159–163.

Barkan, R., Winters, K. B. and McWilliams, J. C. 2017. Stimulated imbalance and the enhancement of eddy kinetic energy dissipation by internal waves. *J. Phys. Oceanogr.* **47**. doi. 10.1175/JPO-D-16-0117.1.

Brekhovskikh, L. M. and Goncharov, V. V. 1994. *Mechanics of Continua and Wave Dynamics*. Cambridge University Press, Springer Verlag, 342 pp.

Chunchuzov, I. 2018. Nonlinear formation of the three-dimensional spectrum of mesoscale wind velocity and temperature fluctuations in stably stratified atmosphere. *J. Atmos. Sci.* **75**, 3447–3467. doi:10.1175/JAS-D-17-0398.1

Chunchuzov, I. P., Vachon, P. W. and Li, X. 2000. Analysis and modeling of atmospheric gravity waves observed in RADARSAT SAR images. *Remote Sens. Environ* **74**, 343–361. doi:10.1016/S0034-4257(00)00076-6

Gjevik, B. and Marthinsen, T. 1978. Three-dimensional lee-wave pattern. *QJ. Royal Met. Soc.* **104**, 947–957. doi:10.1002/qj.49710444207

Gossard, E. E. and Hooke, W. H. 1975. *Waves in the Atmosphere*. New York: Elsevier Scientific Publishing Company, 456 pp.

Johannessen, O. M., Sandven, S., Chunchuzov, I. P. and Shuchman, R. A. 2019. Observations of internal waves generated by an anticyclonic eddy: a case study in the ice edge region of the Greenland Sea. *Tellus A* **71**, 1652881. doi: 10.1080/16000870.2019.1652881

Johannessen, O. M. and co-authors. 1994. Observation and simulation of ice tongues and vortex pairs in the marginal ice zone. In: *The Polar Oceans and Their Role in Shaping the Global Environment, the Nansen Centennial Volume* (ed. O. M. Johannessen, and co-authors) *Geophysical Monograph* 85, Washington, DC: American Geophysical Union, pp. 109–136.

Lighthill, J. 1978. *Waves in Fluids*. Cambridge-London-New York-Melbourne: Cambridge University Press. 504 pp.

Marmorino, G. O., Smith, G. B., North, R. P. and Burkard, B. 2018. Application of airborne infrared remote sensing to the study of ocean submesoscale eddies. *Frontiers Mech. Eng.* 1–10. doi: 10.3389/fmech.2018.00010

Miropolsky, Y. Z. 2001. *Dynamics of the Internal Gravity Waves in the Ocean*. Springer-Science + Business Media B. V., Atmospheric and Oceanographic Sciences Library book series (ATSL, volume 24)

Molemaker, J., McWilliams, J. C. and Capet, X. 2010. Balanced and unbalanced routes to dissipation in an equilibrated Eady flow. *J. Fluid Mech.* **654**, 35–63. doi:10.1017/S0022112009993272

Morison, J. 1986. Internal waves in the Arctic Ocean: A review. In: *The Geophysics of Sea Ice. NATO ASI Series (Series B: Physics)*. Springer, Boston, MA, pp. 1163–1183.

Nagai, T., Tandon, A., Kunze, E. and Mahadevan, A. 2015. Spontaneous generation of near-inertial waves by the Kuroshio Front. *J. Phys. Oceanogr.* **45**, 2381–2406. doi:10.1175/JPO-D-14-0086.1

Nolan, D. S. and Zhang, J. A. 2017. Spiral gravity waves radiating from tropical cyclones. *Geophys. Res. Lett.* **44**, 3924–3931. doi:10.1002/2017GL073572

Plougonven, R. and Zeitlin, V. 2002. Internal gravity wave emission from a pancake vortex: An example of wave-vortex interaction in strongly stratified flows. *Phys. Fluids* **14**, 1259–1268. doi:10.1063/1.1448297

Sandven, S. and Johannessen, O. M. 1987. High-frequency internal wave observations in the marginal ice zone. *J. Geophys. Res.* **92**, 6912–6920.

Shakespeare, C. 2019. Spontaneous generation of internal waves. *Phys. Today* 72, 34–39. doi:10.1063/PT.3.4225

Shakespeare, C., Callum, J. and Taylor, J. R. 2014. The spontaneous generation of inertia-gravity waves during frontogenesis forced by large strain: theory. *J. Fluid Mech.* 757, 817–853. doi:10.1017/jfm.2014.514

Taylor, J. R. and Sarkar, S. 2007. Internal gravity waves generated by a turbulent bottom Ekman layer. *J. Fluid Mech.* **590**, 331–354. doi:10.1017/S0022112007008087

Thomson, W. 1887. On ship waves, Institution of Mechanical Engineers. *Proceedings* **38**, 409–434.

Tunaley, J. K. E. 2012. *The Theory of Internal Wave Wakes*, DRDC Ottawa Contractor Report, CR 2012-119, March.

Wunsch, C. and Ferrari, R. 2004. Vertical mixing, energy, and the general circulation of the oceans. *Ann. Rev. Fluid Mech* 36, 281–314. doi:10.1146/annurev.fluid.36.050802.122121

Appendix

In the case $k\Delta h \gg 1$ we can take $th(k\Delta h) \approx 1$ in Eq. (8) and reduce it to the form

$$\tan(\mu_1 h_1) = \frac{k\mu_1[cth(kh_0)+1]}{[\mu_1{}^2 - k^2 cth(kh_0)]}, \tag{1A}$$

Let us consider Eq. (1A) in case when the stable layer is thin ($\mu_1 h_1 \ll 1$), so that in the left part of (1 A) we can leave only its first term of the expansion by$\mu_1 h_1 \ll 1$ and obtain:

$$h_1 = \frac{k[cth(kh_0)+1]}{[\mu_1{}^2 - k^2 cth(kh_0)]}, \tag{2A}$$

If the bottom depth relative to the stable layer is large ($kh_0 \gg 1$), then in (2 A) we can take $cth(kh_0) \approx 1$ and to write it in the approximate form: $h_1 \approx \frac{2k}{(\mu_1{}^2 - k^2)}$. In the hydrostatic approximation ($|\omega'| \ll N_1$), the expression for $\mu_1{}^2$ can be approximated as follows

$$\mu_1{}^2 \approx k^2 N_1{}^2/\omega' 2 = k^2 N_1{}^2/k_x{}^2 V^2 = (g\varepsilon/h_1)/(k^{-2} k_x{}^2 V^2), \tag{3A}$$

where $\varepsilon \equiv -\Delta\rho/\rho$ is the absolute value of the relative density jump within the thin layer with $N = N_1$, therefore (11) is reduced to the form: $h_1 \approx \frac{2k}{\mu_1{}^2} \approx \frac{2kh_1}{g\varepsilon} V^2 k^{-2} k_x{}^2$, from which we obtain the equation

$$V^2 k_x{}^2 = g\varepsilon k/2 \tag{4A}$$